

A Highly Sensitive Triboelectric Vibration Sensor for Machinery Condition Monitoring

Hongfa Zhao, Mingrui Shu, Zihao Ai, Zirui Lou, Kit Wa Sou, Chengyue Lu, Yuchao Jin, Zihan Wang, Jiyu Wang,* Changsheng Wu, Yidan Cao, Xiaomin Xu, and Wenbo Ding*

Vibration sensors are involved extensively in a variety of applications. Especially in the era of the Internet of Things, developing self-powered vibration sensors has become a very meaningful yet challenging problem. This study investigates a highly sensitive self-powered vibration sensor based on the triboelectric nanogenerator (VS-TENG) for machinery condition monitoring. By introducing a stacked structure comprising foamed aluminum, and a fluorinated ethylene propylene film with gold-plated electrode protected by two indium tin oxide layers, The VS-TENG can detect the vibrations with frequencies ranging from 1 to 2000 Hz and can detect vibrations of low amplitude (approximately sub- μm , by calculation). The output performance and characteristics of the TENG under various vibration frequencies, accelerations, and amplitudes are analyzed systematically. The VS-TENG is successfully used to monitor the operating conditions of mechanical gear systems, reaching a recognition accuracy of 99.78%. Furthermore, it can also be utilized for vibration detection in other areas such as the air compressor, heat gun, hollow tile recognition, etc., which means a solid progress toward the practical applications of TENGs in self-powered vibration detection.

1. Introduction

Vibration sensors are widely used in the fields of infrastructure health, vehicle safety, biomedical equipment, intelligent electronic products, mechanical equipment vibration monitoring.^[1–4] However, new challenges have shown up with the booming development of Internet of Things (IoT) and sensor networks,^[5–7] especially in scenarios where extensive sensing/monitoring is required yet in situ power supply is not easily accessible (which impedes the deployment of traditional sensors).^[8,9] One appealing alternative to this problem is to develop self-powered sensors, of which self-powered vibration sensing is an important subject.^[10–13]

At the same time, with the development of the IoT, machinery and equipment are evolving toward more automation, higher intelligence, and better efficiency.^[14] For example, unmanned ships can undertake large-scale, long-term, low-cost missions, with great implications in both commercial and security sectors. However, mechanical equipment is expected to operate stably for a long time, and its operating condition should be monitored in real time.^[15,16] Once the operating state gets abnormal, measures need to be taken immediately. The sensors may be frequently exposed to harsh environments with high temperature and high humidity.^[17,18] Furthermore, considering the cost and power consumption of the sensors in a broader sense, the sensor needs to work normally even in a power system failure. In this sense, self-powered vibration sensors have unique advantages.^[19]

Based on the contact electrification and electrostatic induction, triboelectric nanogenerators (TENGs) can effectively convert mechanical energy into electrical energy, proved their potential in energy harvesting and self-powered sensing.^[20–25] Therefore, TENG-based vibration sensors have received wide attention due to the high sensitivity and excellent output performance.^[26–29] Recent advances in TENG have demonstrated its application in monitoring railway vibration,^[30] wind blower,^[31] marine equipment,^[32] bridge,^[26] automotive engine,^[1] etc.^[2,16,17] These TENG-based vibration sensors use either a spring-mass system,^[1,30–31,33] sliding block^[26] or ball bouncing,^[32] and thus need to overcome the weight of the heavy vibration components during operation. Their frequency detection usually ranges in tens or hundreds of hertz, and their detectable


H. Zhao, Z. Ai, Z. Lou, K. W. Sou, C. Lu, Y. Jin, Z. Wang, J. Wang, Y. Cao, X. Xu, W. Ding
Tsinghua-Berkeley Shenzhen Institute
Shenzhen International Graduate School
Tsinghua University
Shenzhen 518055, P. R. China
E-mail: jiyuwang@sz.tsinghua.edu.cn; ding.wenbo@sz.tsinghua.edu.cn

M. Shu
Southern Marine Science and Engineering
Guangdong Laboratory (Guangzhou)
Shenzhen Key Laboratory of Marine IntelliSense and Computation
Shenzhen International Graduate School
Tsinghua University
Shenzhen 518055, P. R. China

C. Wu
Department of Materials Science and Engineering
National University of Singapore
9 Engineering Drive 1, Singapore 117575, Singapore

Y. Cao, X. Xu
Shenzhen Geim Graphene Center
Institute of Materials Research
Tsinghua Shenzhen International Graduate School
Tsinghua University
Shenzhen 518055, P. R. China

W. Ding
RISC-V International Open Source Laboratory
Shenzhen 518055, P. R. China

 The ORCID identification number(s) for the author(s) of this article can be found under <https://doi.org/10.1002/aenm.202201132>.

DOI: 10.1002/aenm.202201132

amplitude usually ranges in millimeter. One of the sensors can detect a minimum vibration amplitude of 3.5 μm but only under the resonance state.^[31] However, under low-amplitude vibrations, overcoming the structural weight can be difficult, and the spacing between the tribocharge layers cannot change effectively. In this case, the TENG output gets reduced (if not totally negligible), and the waveform is easily distorted (i.e., different from that of the vibration source). Therefore, it remains challenging to design self-powered vibration sensors capable of detecting wider frequency range and lower amplitude (sub- μm) vibrations to improve the machinery monitoring accuracy and expand their application.

In this study, we have developed a highly sensitive self-powered vibration sensor based on triboelectric nanogenerator (VS-TENG). The triboelectric layer is composed of a foamed aluminum and a fluorinated ethylene propylene (FEP) film with one side gold-plated for the electrode. The lightweight FEP film can vibrate freely with the source of excitation, while the foamed aluminum with a porous structure can effectively increase the contact area and reduce the air damping applied on the vibration film. This fabricated TENG can detect the vibrations with frequencies ranging from 1 to 2000 Hz and vibrations of low amplitude (approximately sub- μm , by calculation). Even in the high temperature and high humidity environment, the electrical signals of TENG still yield high consistency with the excitation waveform (including frequencies, only amplitude may change). With a recognition accuracy of 99.78%, it has been primarily applied in monitoring the operation of mechanical gear systems. The results can be displayed on both remote monitoring devices and other mobile applications. The VS-TENG can also be utilized for vibration detection in other areas such as the air compressor, heat gun, hollow tile recognition, etc., with the data processed by an embedded system and displayed on a local screen. This work indicates a substantial progress toward the practical applications of TENGs in self-powered vibration detection.

2. Results and Discussion

2.1. Structure and Working Principle of the VS-TENG

A schematic diagram of the application of studied vibration TENG is shown in **Figure 1a**. The VS-TENG can detect vibrations of machinery as well as vibrations of infrastructures in industries and daily lives. The signals output by the TENG can be transmitted to the server via a wireless network. After processing, the result can be displayed on computers or handheld mobile devices. In this case, the operating conditions of the detected equipment can be monitored continuously in real-time. The photos and structure scheme of the TENG are shown in **Figure 1b,c**. The TENG is circular shaped, while the radius of the effective working area is 15 mm. It consists of a foamed aluminum as both the electrode and tribocharge layer, an FEP film as another tribocharge layer with a gold-plated electrode (100 nm), and a paper with the thickness of 0.1 mm to separate the two tribocharge layers. Note that the surface of the FEP film is uneven (**Figure 1d**) so that a larger contact area may be achieved when contacting and separating with the foamed

aluminum, which is helpful for achieving larger electrical output from contact electrification.^[34] An air cavity is formed between the FEP and the foamed aluminum, and the porous structure (**Figure 1e**) of the foamed aluminum material can connect the cavity with the outside air so that the air will not greatly damp the two materials during the process of contact/separation. Furthermore, two transparent indium tin oxide (ITO) membranes with polyethylene terephthalate (PET) substrates (ITO 10 μm , PET 115 μm) are fixed above and below the TENG respectively to protect the internal structure and exhibit a specific function of the electrostatic shielding effect (the functions of the ITO and paper materials will be detailed in Note S1, Supporting Information). To reduce interruption to the vibration of the flexible film, air holes are punched on the ITO membranes to balance the internal and external air pressure, allowing the alternating airflow generated during the vibration to circulate freely.

Figure 1f depicts schematically the working mechanism of the VS-TENG. When the TENG is forced to move under the excitation of the vibration source, the FEP film is subject to alternating air resistance, which induces periodic changes in the pressure between the FEP film and the foamed aluminum, causing the FEP film to oscillate repeatedly and lag behind the vibration phase. When the FEP film gets in contact with the foamed aluminum, the electron clouds on the surfaces of the two films overlap, and some of the electrons from the aluminum enter the deeper potential well of the FEP film.^[35,36] Due to the much higher electronegativity of FEP than aluminum, the free electrons on the surface of the aluminum transfer to the lowest unoccupied molecular orbital of the FEP interface,^[36] so the FEP film becomes negatively charged while the aluminum becomes positively charged (**Figure 1f(i)**). Since the air pressure on the FEP film is always opposite to the direction of vibration, the FEP film will be subjected to downward air resistance and come into contact with aluminum when the vibration source moves upward (**Figure 1f(ii)**). At this moment, electrons are obtained by the FEP film from aluminum, and current flows from the gold electrode to the aluminum via an external circuit. Conversely, when the vibration source moves downward, the FEP film will separate from the aluminum and current flows from the aluminum to the gold electrode due to the potential difference of the local electric field (**Figure 1f(iv)**). Finally, the FEP film returns to the original position, with the electric charge distribution returning to its initial state (**Figure 1f(i)**), and an entire cycle of electricity generation has been completed. The working principle of the HR-TENG is further confirmed in **Figure 1g**, which demonstrates the simulation results of the potential distribution between the FEP film and foamed aluminum obtained by COMSOL software. Thus, an alternating current pulse is generated as the output of the VS-TENG.

2.2. The Output Performance and Characteristics of the TENG under Different Vibration Conditions

To analyze the output performance and characteristics of the VS-TENG systematically, a vibration exciter capable of generating arbitrary vibrations in 1–2000 Hz is used in the experiments as shown in **Figure 2a**. The experiment process is illustrated in **Figure 2b**. First, a signal generator is used to

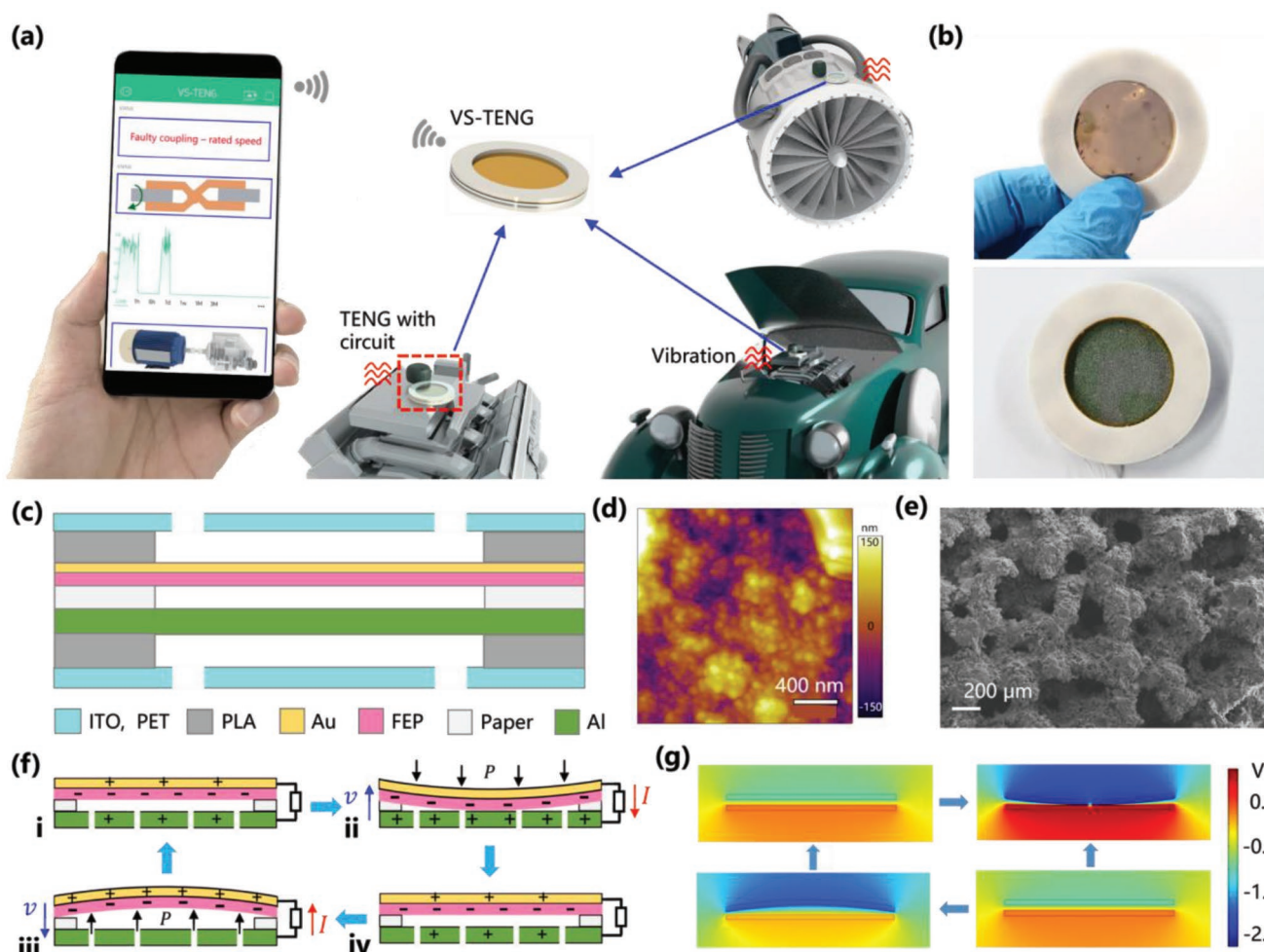


Figure 1. Structure and working principle of the TENG. a) Schematic diagram of the application of the VS-TENG. b) Two photographs of the TENG. c) Structural scheme of the TENG. d) Surface topography image of the FEP film scanned by an atomic force microscope. e) SEM image of the surface of foamed aluminum. f) Working mechanism of the TENG. g) COMSOL simulation of the periodic potential change between the two electrodes of the HR-TENG.

generate sinusoidal signals of different frequencies, which will be amplified by a power amplifier to drive the exciter to vibrate. The FEP film of TENG vibrates with the exciter and converts mechanical vibrations into electrical signals. It should be noted that the FEP film has different vibration modes at different frequencies. The first and the second vibration modes from the simulation are shown in Figure 2a, and the third to fifth vibration modes are shown in Figure S1 (Supporting Information). In these frequency ranges, the FEP film is in resonance and hence produces a larger displacement, thus, the TENG may generate a higher electrical output. Combining with the analysis of the working principle of the VS-TENG, the vibration characteristic of the FEP film can be expressed as

$$x(t) = \frac{F_0}{m \sqrt{(\omega_0^2 - \omega^2)^2 + 4 \left(\frac{m^2}{\alpha^2} + \omega^2 \right)}} \cos(\omega t - \varphi) \quad (1)$$

where $x(t)$ is the displacement amplitude of the FEP film, F_0 is the force exerted by the vibration source, m is the mass of the

FEP film, α is the damping coefficient from the air, ω and ω_0 are the angular frequencies of the vibration source and that of the FEP film, respectively.

The electrical output of the TENG is measured by the electrometer, which sends the signals to the computer. (Note that the signals directly measured by the electrometer are not purely signals representing vibration but a mixture of vibration signals and environmental interferences.) After filtering the noise out, the signals reflecting the actual vibration output by the TENG can be obtained and displayed on the screen. The voltage signal output by the TENG (when the vibration frequency of the exciter is 200 Hz) and the corresponding spectrum are shown in Figure 2c,d.

It can be seen that frequency-domain signals output by the TENG are mainly concentrated in 200 Hz (dominant frequency), 50 Hz (corresponding to the environmental interference), 400 and 600 Hz (harmonics output from the TENG during the vibration process, see Figure 2d). Obviously, the dominant frequency signal output by the TENG distinguishes itself in that it has a much larger magnitude than its harmonics, which is an important advantage compared with

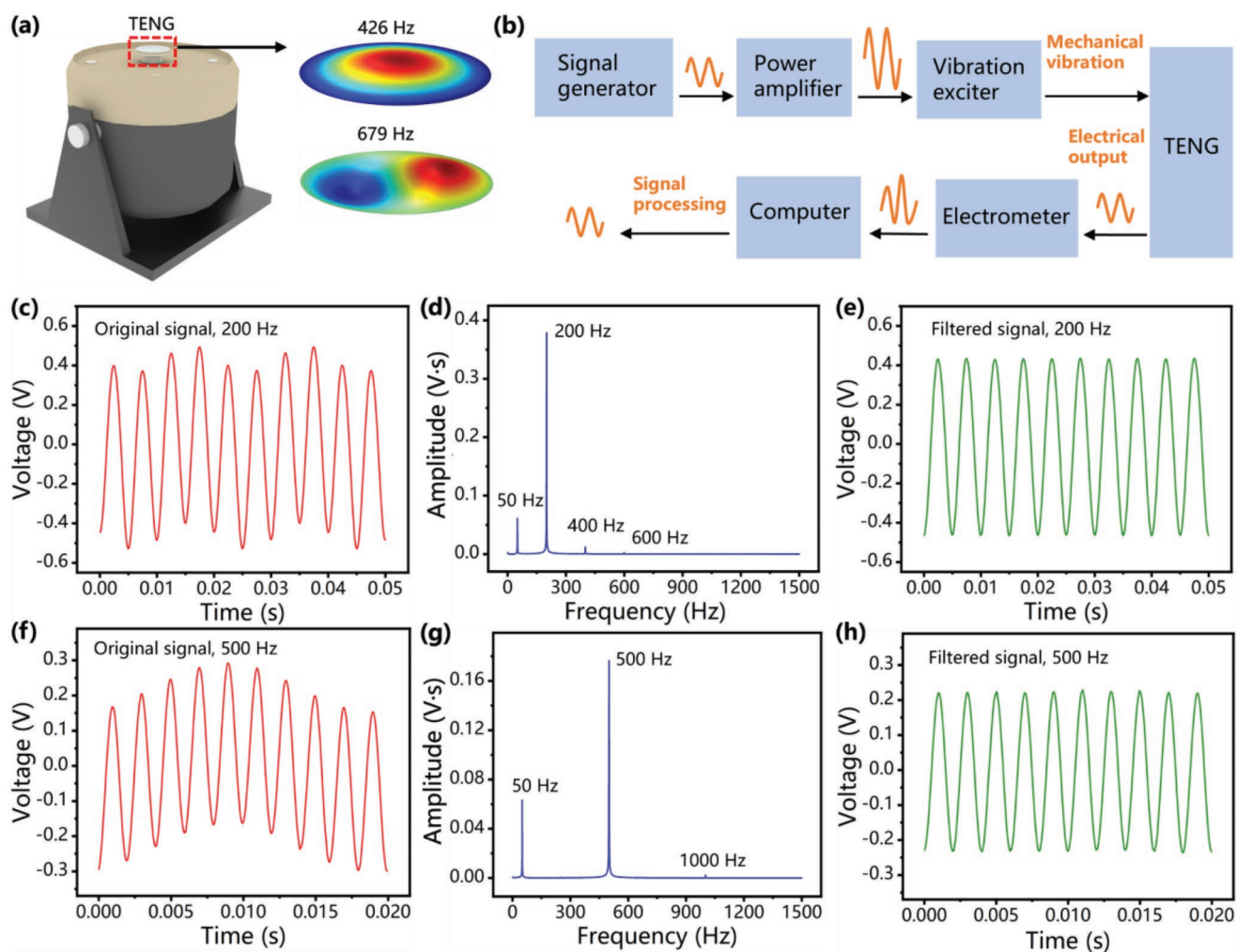


Figure 2. The experiment process and output performance of the TENG. a) Schematic diagram of the experiment device and vibration modes of the TENG. b) The flow chart of the experiment. c) The original signal of the TENG at a vibration frequency of 200 Hz. d) The Fourier transform of the voltage signal and e) the voltage signal after filtering out 50 Hz noise from (c). f) The original voltage output by the TENG at a frequency of 500 Hz. g) The Fourier transform of the voltage signal and h) the voltage signal after filtering out 50 Hz noise from (f).

piezoelectric vibration sensors.^[17] After filtering out the 50 Hz noise from the environment, the actual voltage signal output by the VS-TENG is shown in Figure 2e. Similar results can be obtained after analyzing the voltage signal of the TENG at a frequency of 500 Hz and directly measured by the electrometer (Figure 2f). The harmonic signal concentrating on 1000 Hz is much smaller than the dominant frequency signal (Figure 2g), and the periodic sinusoidal signal can be obtained after 50 Hz filtering (Figure 2h), the filters used in the experiments are all digital ones). The voltage signals output by the VS-TENG at 500, 1000, 2000 Hz and their Fourier transform are shown in Figures S2–S4 (Supporting Information). It is worth to note that the porous structure of the foamed aluminum is very important for the electrical output of the TENG. The output performance of the TENG with foamed aluminum is much better than that with the normal aluminum (details are shown in Note S2, Supporting Information).

Vibration frequency, acceleration, and displacement are the most commonly used physical quantities for vibration

characterization. For sinusoidal vibrations, the relationships between these parameters are

$$x(t) = A \sin(\omega t) \quad (2)$$

$$\alpha(t) = B \sin(\omega t) \quad (3)$$

$$B = A\omega^2 \quad (4)$$

where $x(t)$ is the displacement, ω is the angular frequency, A is the displacement amplitude, $\alpha(t)$ is vibration acceleration, and B is the amplitude of acceleration. In this way, when the vibration frequency is fixed, the acceleration can be measured by the accelerometer, thereby calculating the displacement amplitude.

The schematic diagram for the relationship among vibration frequency, acceleration, and displacement amplitude is shown in Figure 3a. The red and orange points are respectively the vibration parameters for Figure 3b,c, and it should be noted

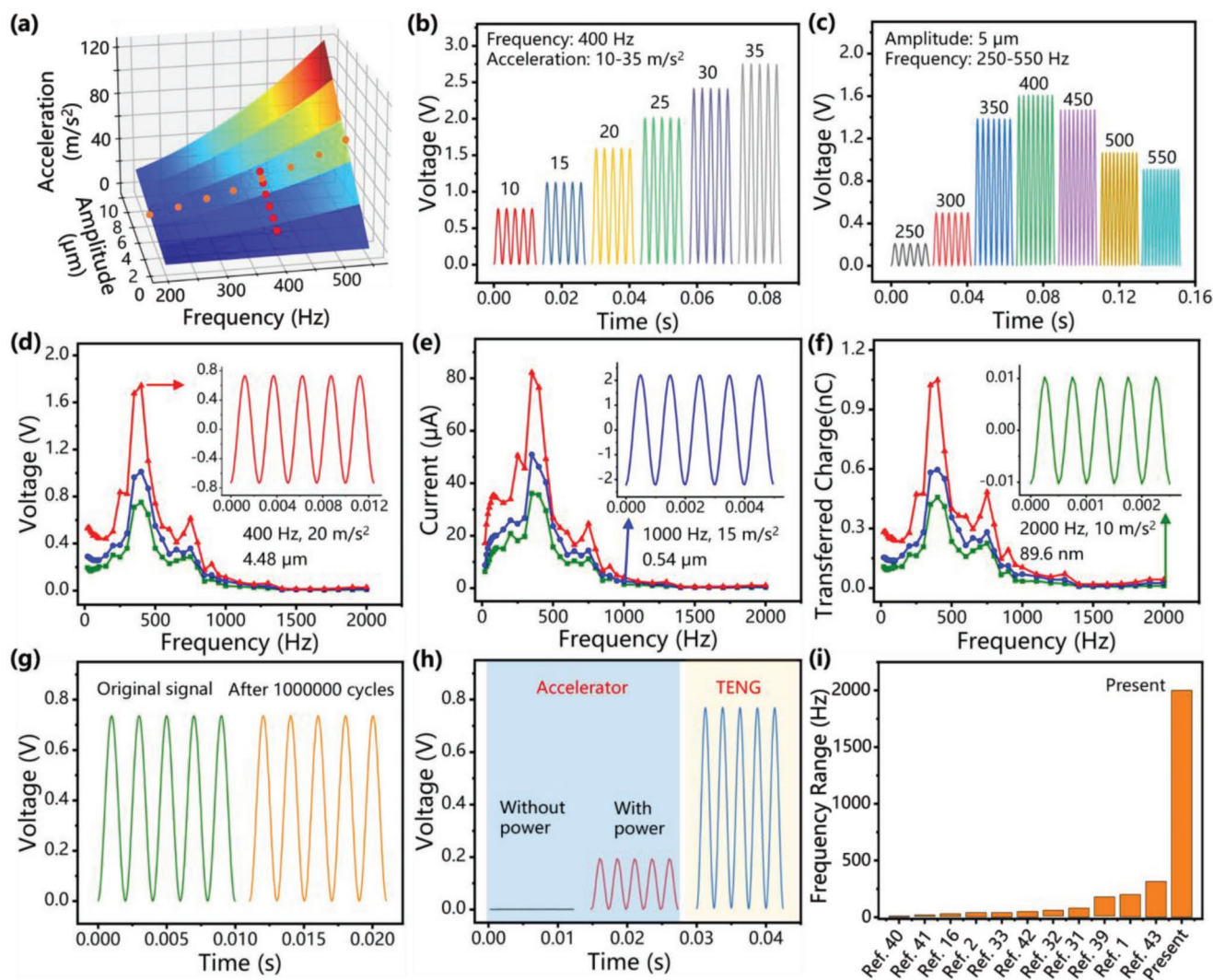


Figure 3. The output performance and characteristics of the VS-TENG under different vibration conditions. a) Relationship among vibration frequency, acceleration, and displacement amplitude. Variation of the open-circuit voltage output by the VS-TENG with b) different accelerations from 10 to 35 m s^{-2} at a fixed frequency of 400 Hz and c) different frequencies from 250 to 550 Hz at a fixed amplitude of 5 μm . d) Open-circuit voltage, e) short-circuit current, and f) transferred charge of the VS-TENG under the excitation of vibration with frequencies ranging from 20 to 2000 Hz. g) Comparison of the original signal and the voltage signal after working 1 000 000 cycles from VS-TENG. h) Comparison of the voltage signals output by the VS-TENG and a commercial accelerometer. i) Comparison of the VS-TENG and other TENGs for vibration sensing, demonstrating the widest frequency range.

that these are the theoretical parameters for the vibration source but not the electrical output of the TENG. Consistent with Equation (4), the acceleration is proportional to the displacement amplitude and proportional to the square of the frequency. In the experiment, the vibration acceleration is measured by an accelerometer provided by the same manufacturer as the vibration exciter, the vibration frequency is controlled by the signal generator, and thus the vibration amplitude can be calculated according to Equation (4). Figure 3b shows the open-circuit voltage signals output by the VS-TENG with different accelerations from 10 to 35 m s^{-2} at a fixed frequency of 400 Hz (the voltage signals are processed above the zero line, and signals for other frequencies are shown in Figure S5, Supporting Information). The VS-TENG has output voltages of about 0.78, 1.15, and 2.76 V at 10, 15, and 35 m s^{-2} , respectively, meaning that the output voltage of the VS-TENG has a good

linear relationship with vibration accelerations (Figure S6, Supporting Information). Figure 3c shows the open-circuit voltage signals (signals for short-circuit current and transferred charge are shown in Figure S7, Supporting Information) with different frequencies from 250 to 550 Hz at a fixed amplitude (vibration source) of 5 μm , demonstrating that the output voltage varies with the frequency and reaches a peak value at ≈ 400 Hz (the displacement of the FEP film should be maximum around this frequency).

The open-circuit voltage, short-circuit current, and transferred charge output by the VS-TENG at three different vibration accelerations with frequencies ranged from 20 to 2000 Hz are also systematically analyzed (Figure 3d–f). To filter out environmental noise and get the actual electrical signals output by the TENG, a bandpass filtering is performed for specific frequencies, and then the peak values of the electrical signals are

calculated (the instantaneous signals for all points are shown in Figures S8–S16, Supporting Information). The instantaneous signals after filtering at frequencies of 400, 1000, and 2000 Hz are shown in Figure 3d–f, demonstrating regular sinusoidal signals. The red, blue, and green curves represent the peak values of the electrical signals output by the VS-TENG at acceleration rates of 15, 10, and 5 m s^{-2} , respectively. Those electrical signals have the same trend, that is, reaching the first peak at $\approx 400 \text{ Hz}$ (instantaneous signals around 400 Hz are shown in Figure S17, Supporting Information), and the second smaller peak at $\approx 750 \text{ Hz}$. The FEP film vibration also shows comparable simulation results (Figure 2a; Figure S1). For the instantaneous signals in Figure 3d–f, with the known variables of frequency and acceleration, the vibration amplitude can be calculated as $4.48 \mu\text{m}$, $0.54 \mu\text{m}$, and 89.6 nm (calculation details are shown in Note S3, Supporting Information), demonstrating that the VS-TENG can detect low-amplitude vibrations. And for each point, their main vibration parameters are determined. It should be noted that the working principle of the TENG is based on both contact triboelectrification and electrostatic induction, even in the low amplitude vibration conditions, the VS-TENG can also work stably (detailed explanation are shown in Note S4, Supporting Information).

The VS-TENG can also detect the vibration in the lower frequency range of 1–20 Hz, and the voltage signals output by the TENG at the frequencies of 1, 10, and 15 Hz are shown in Figure S18 (Supporting Information). Since the linear motor works well in low frequencies and is often used for vibration studies, additional experiments are added to detect the vibration from 1 to 5 Hz using a linear motor (Figure S19, Supporting Information). The data in this range are not demonstrated along with the data in 20–2000 Hz range because the amplitude difference is too large. Under the same acceleration, the amplitude for 1 Hz is 4 million times larger than that for 2000 Hz. The continuous frequency response of the sensor by sweeping frequency is compared in Note S5 of the Supporting Information. The vibration in the above experiments are all vertical experiments, while the VS-TENG can also detect the vibration in other directions, the experiments and signals are shown in Figures S20 and S21 (Supporting Information), which broaden the application scenarios of the VS-TENG. It is worth noting that the electrical output of the VS-TENG will decrease with the increased temperature, while the waveform of electrical signals remains constant (Note S6, Supporting Information). And humidity does not have a significant effect on the VS-TENG, when the humidity increases, the electrical output of the VS-TENG will only increase slightly, indicating high stability under different humidity. Moreover, the demonstration of the experiment and voltage signals output by the VS-TENG is shown in Movie S1 of the Supporting Information, in which the signals are filtered out 50, 250, and 500 Hz (power frequency interference and its harmonics). In the real-time demonstration, the voltage can be calculated directly, and the frequency is obtained by the Fourier transform, thus we can get the vibration acceleration and furtherly the vibration amplitude (see Note S7, Supporting Information). Since the TENG has different sensitivities at different frequencies, the waveform of the voltage signal may be different from that of the vibration acceleration. This can be solved by an algorithm, which provides a method for the

interconversion between TENGs complex electrical signals and the vibrations from the source (the details shown in Note S8, Supporting Information).

In addition, the VS-TENG exhibits high durability, after working for 1 000 000 cycles, the voltage signals output by the TENG has no obvious difference from the initial signals (Figure 3g, the experimental process is shown in Note S9, Supporting Information). Compared with the commercial piezoelectric accelerometer, the TENG can perform sensing work normally without a power supply, and its electrical output is higher than that of the piezoelectric sensor (Figure 3h). Previous studies have made significant progress in vibration detection using TENGs.^[2,14,17,26–28,31–32,37–43] Compared with the relevant studies on TENGs for vibration sensing, the VS-TENG shows a good performance for detecting a wider frequency range and lower amplitudes (Figure 3i; Table S1, Supporting Information). There are also other TENG-based vibration sensors applied in different areas, such as the TENG sensor system that can detect vibrations in underwater environments and send signals wirelessly,^[44] the TENG sensor detecting the impulse vibration from steel balls or hands striking a wood plate,^[45] and bionic membrane sensor that can detect pulse and laryngeal vibrations in a wide frequency band,^[46] demonstrating the great potentials of TENGs for vibration detection.

2.3. Machinery Condition Monitoring with the VS-TENG

Figure 4a shows the schematic diagram of the machinery condition monitoring with the VS-TENG. A gear box driven by a motor is used as the vibration source. The VS-TENG is placed on the top of the gearbox to convert the mechanical vibrations into electrical signals, which are subsequently detected by an acquisition board and sent to the computer by the ESP-32 circuit board via WiFi. In this way, the data can be collected and displayed on the screen in real-time. At first, the vibrations of the gearbox in normal operation without any faults are detected by the VS-TENG, and the instantaneous voltage signals output by the TENG at different rotary speeds are shown in Figure 4b. Obviously, the gearbox produces stronger vibration at higher speeds. Thus, TENG outputs a higher voltage signal, and the voltage signals for the entire duration are shown in Figure S22 (Supporting Information). The spectrums are obtained after performing Fourier transform on these signals, shown in Figure 4c–e. For the low-speed rotation, the central frequencies are 124 and 151 Hz. And for the medium-speed rotation, the central frequency concentrates on 391 Hz. But when the gearbox is in high-speed rotation, more characteristic frequencies appear; the frequencies mainly concentrate at 361, 651, and 838 Hz. Therefore, under different operating speeds of the gearbox, the signals output by the VS-TENG have apparent differences in both the time and frequency domains. The spectrums up to 5000 Hz are shown in Figure S23 (Supporting Information), notice that there are still frequency-domain signals in 2000–2500 Hz, which means that the response frequency band of the VS-TENG is larger than 2000 Hz.

However, when the rotational speed is the same and other operating conditions (reverse rotation, shaft misalignment, and faulty coupling) are changed, it is difficult to recognize the

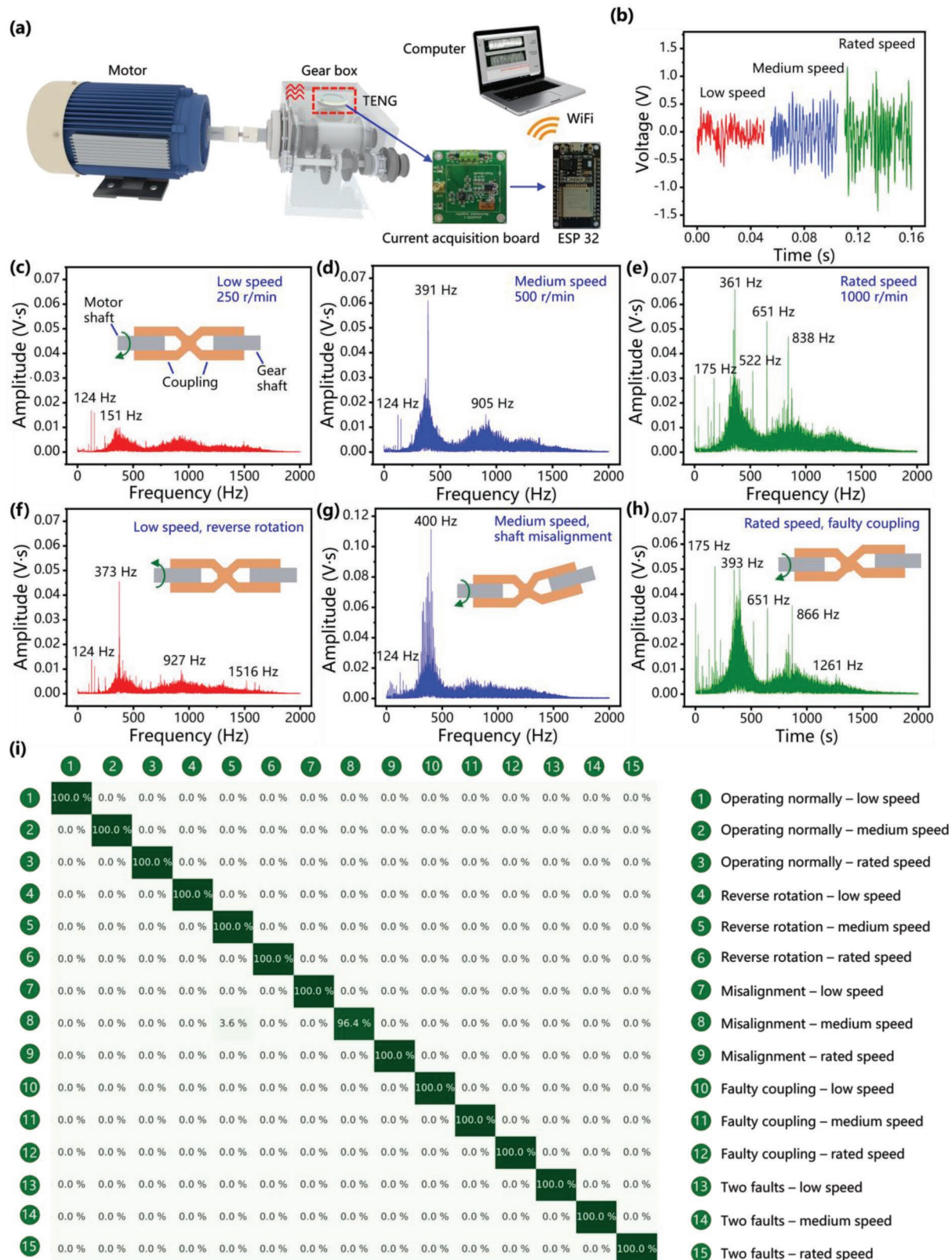


Figure 4. Machinery condition monitoring with the VS-TENG. a) Schematic diagram of the experiment. b) Instantaneous voltage signals output by the TENG at different rotational speeds of the gearbox. Spectrum of the voltage signals output by the TENG with the gearbox in c) low rotational speed, d) medium rotational speed, e) rated rotational speed, f) low rotary speed and reverse rotation, g) medium rotational speed and shaft misalignment, and h) rated speed and faulty coupling. i) The confusion matrix of the deep learning outcome for recognizing the gearbox operating conditions.

difference between the time-domain signals intuitively. In this situation, the frequency-domain signals need to be analyzed and compared. When the gear box operates in low-speed and reverse rotation, the frequency-domain signal (Figure 4f, original signals with all speeds and Fourier transform with other speeds) changes significantly compared with that in low-speed and forward rotation condition (Figure 4c), with more characteristic frequencies and the main frequency shifting to 373 Hz. While in medium-speed and shaft-misalignment condition, the spectrum (Figure 4g, original signals with all speeds and Fourier transform with other speeds) also shows differences in Figure 4d, with more characteristic frequencies around 400 Hz, and a higher amplitude for the main frequency, which means stronger vibration in this case. Furthermore, when the gearbox operates at a rated-speed with a faulty coupling, the spectrum (Figure 4h, original signals with all speeds and Fourier transform with other speeds) shows both similarities and differences in Figure 4e, with some characteristic frequencies changing (393, 866 Hz) and some remained (522, 651 Hz).

In the research field of mechanical fault diagnosis, it has been proved that intelligent fault diagnosis techniques may replace time-consuming and unreliable human analysis, increasing the efficiency of fault diagnosis.^[47,48] Above discussions show that the mechanical vibration can be detected by the VS-TENG and the vibration details are all reflected in the time-domain signals and frequency-domain signals. The voltage signals output by the VS-TENG under 15 different vibration conditions are collected. After applying a neural network algorithm on these signals, new data generated from different vibration conditions can be recognized with the learning result. The confusion matrix of the machine learning result shows an accuracy of 99.78% for identifying the gearbox's operating conditions, indicating that the VS-TENG is an accurate sensor for machinery condition monitoring. The vibration of the gearbox can also be detected by the VS-TENG with the result displayed on a computer screen and mobile device in real-time (Movie S2, Supporting Information).

2.4. Vibration Detection for Other Devices with the VS-TENG

A photograph of the experiment for detecting the compressor vibration with the VS-TENG is shown in Figure 5a. The TENG is placed on the top of the compressor, and different vibration characteristics will be produced when the compressor is in starting, operating, and closing phases. As a result, the VS-TENG output different voltage signals when detecting on different operating phases (Figure 5b). The spectrum is obtained after the Fourier transform of the voltage signals during the operating phase of the compressor (Figure 5c), which is much different from that during the compressor's starting and closing phases (Figure S30, Supporting Information). Moreover, the compressor operating vibration can be detected by the VS-TENG with the data processed by an embedded system in real-time and the result will be displayed on the local screen (Movie S3, Supporting Information).

The VS-TENG can be used to detect the vibration of the heat gun as well (Figure 5d). When the heat gun operates at low speed or high speed, the TENG output different signals (Figure 5e), and the comparison of the spectrums after Fourier transform for these two signals is shown in Figure 5f. The voltage is higher when the heat gun operates at low speed with a central frequency of 100 Hz. The central frequency increases to 280 Hz when the heat gun operates at high speed while the amplitude decreases. That is because the vibration frequency of the heat gun increases with the rotational speed, while the vibration displacement decreases with the improvement of the frequency.

It should be noted that for electrical equipment, the current change rate in the circuit is the largest at the moment of power-on, power-off or change of operating state. Under the impact of this strong current, the electrical equipment will also have instantaneous high-amplitude vibration. Therefore, in Figure 3b,e, when the operating state of the detected device changes, the voltage output of the TENG also changes abruptly. For the air compressor, when it is turned on, the cylinder valve is closed so that the motor runs with load, while it is turned off, the cylinder valve is opened for exhaust. Therefore, the air compressor generates stronger vibration at the moment of closing than at the moment of opening, so the voltage output of the TENG changes more significantly. When mechanical equipment is operating, its mechanical components may vibrate with different frequencies so that complex mechanical systems often generate complex vibrations. After Fourier transform, the spectrogram of the vibration signal from the compressor will be more complicated than that from the heat gun. By analyzing the signal output by the TENG, the vibration details of the mechanical equipment can be obtained, so as to estimate whether the vibration of the mechanical equipment is normal.

In addition, TENG can also be used to identify the laying condition of floor tiles (Figure 5g). Compared with the normally laid tiles, the vibration generated by the hollow brick when struck by the hollow hammer is significantly enhanced, and the vibration duration increases, so the voltage signal output by the TENG is significantly different.

3. Conclusion

In summary, a highly sensitive self-powered vibration sensor based on the TENG is fabricated and studied. The VS-TENG is composed of a foamed aluminum, an FEP film with one side gold-plated as the electrode, and two ITO membranes as the protection lies. The foamed aluminum with a porous structure can effectively increase the contact area and decreases the air damping applied on the vibration film. The VS-TENG can detect the vibrations with frequencies ranging from 1 to 2000 Hz and can detect vibrations of low amplitude (approximately sub- μm , by calculation). The output performance and characteristics of the TENG under different vibration frequencies, accelerations, and amplitudes are analyzed systematically. The electrical output of the VS-TENG can be influenced by the temperature and humidity, but the waveforms of the signals remain unchanged, indicating high stability under a high-temperature and high-humidity environment. Especially, it has

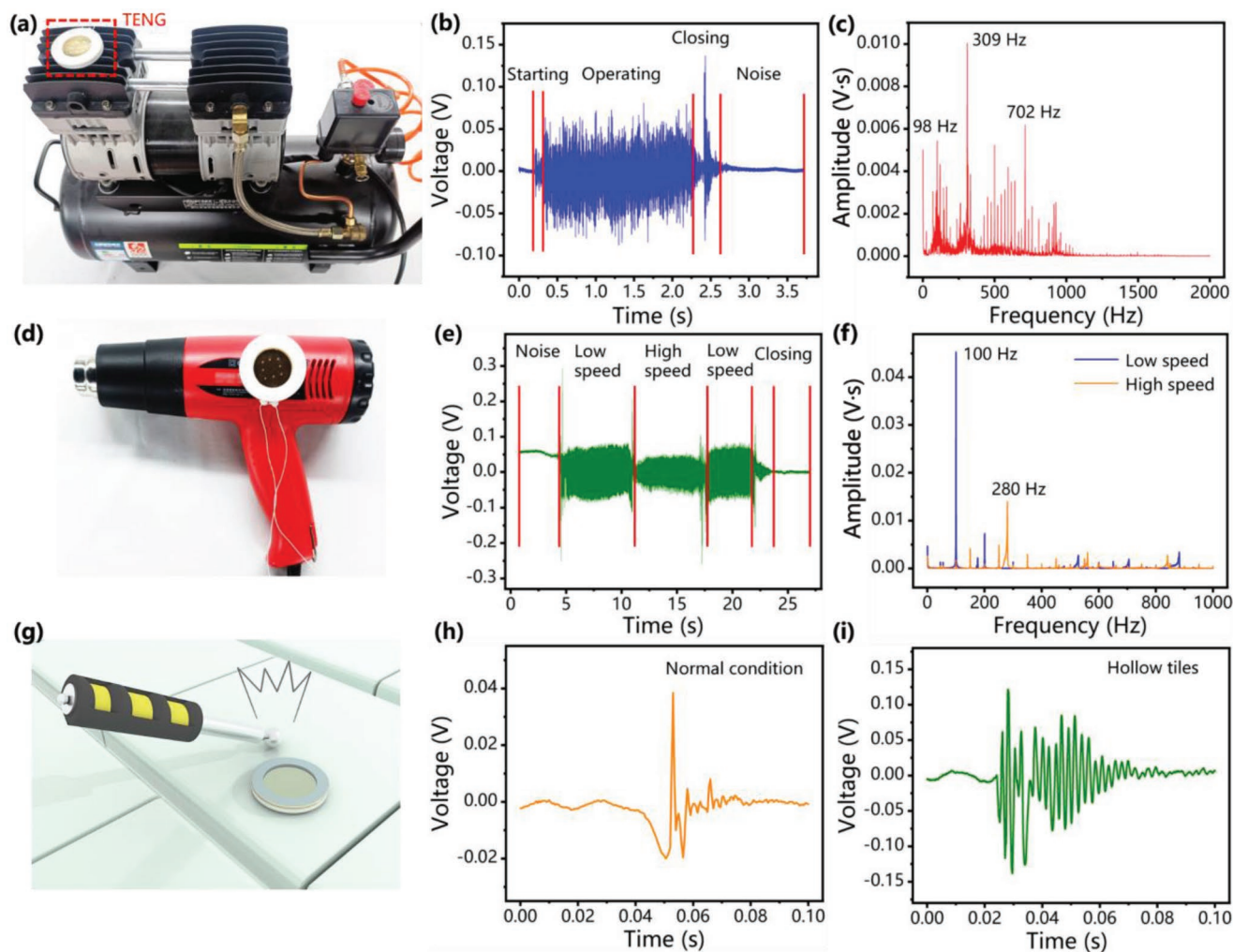


Figure 5. Vibration detection for actual machines with the VS-TENG. a) Photograph of the experiment for detecting the compressor vibration. b) Voltage signals output by the TENG for detecting the operation of the compressor. c) Fourier transform for the voltage signals during compressor operating. d) Photograph of the experiment for detecting the vibration of a heat gun. e) Voltage signals output by the TENG for detecting the operation of the heat gun. f) Frequency domain obtained by Fourier Transform of the voltage signals during low-speed and high-speed operation. g) Schematic diagram of the hollow tile detection. Voltage signals output by the TENG when detecting the h) normal tile and i) hollow tile.

been successfully applied to monitor the operating conditions of mechanical gear systems with a recognition accuracy of 99.78%. The results can be displayed on both the computer screen and other mobile devices. Furthermore, it can be used for vibration detection in other areas such as the air compressor, heat gun, hollow tile recognition, etc. The detected data is further processed by an embedded system and displayed on the local screen. This work presents solid progress toward the practical applications of TENG in vibration detection and has great potential for the development of self-powered vibration sensing.

4. Experimental Section

Fabrication of the VS-TENG: The VS-TENG consists of a foamed aluminum, an FEP film with a gold-plated electrode, and a paper (3M adhesive tape) with a thickness of 0.1 mm to make the two tribocharge layers have a certain distance. The FEP film was used as the electronegative triboelectric layer due to its strong electronegativity

and good flexibility. It has a thickness of 50 μm , and its surface is sanded by a sandpaper (10 000 meshes per unit area) to make surface microstructures and increase the surface potential. Given that the FEP material is insulated, a gold electrode (deposited by a thermal evaporation) with a 100 nm thickness is attached to the backside of the FEP film to transfer electrons. The diameter of the effective working area of the TENG is 15 mm. The shell of the TENG is printed by a 3D printer (Raise 3D Pro2 Plus) with PLA material, and its diameter is 25 mm. Two transparent ITO films (0.1 mm, each with 10 air holes) are fixed above and below the TENG respectively to protect the internal structure.

Experimental Process and Measuring Equipment: When measuring the electrical output of the VS-TENG, the device was mounted on an electrodynamic shaker (SA-JZ010), which was driven by an amplified sinusoidal wave from a function generator (SA-SG030) and an amplifier (SA-PA020). For the data in Figures 2, 3, and 5, the output signals, including the open-circuit voltage, short-circuit current, and transferred charges, were measured by Keithley 6514 electrometer. The MATLAB interface in LABVIEW was used to process and display the real-time signals measured with the electrometer. The model of the accelerometer provided by the exciter manufacturer in the experiment was SACL201LYTE. For the data of Figure 4, the output signals were

measured by a current acquisition board, and the signals were sent to a computer in real time by ESP-32 circuit board (with a sampling frequency of 20 000 Hz) through WiFi. An adding device was connected between the current acquisition board and ESP-32 due to that the ESP-32 was not able to send negative data to the computer. The rated speed of the motor in the experiment was 1000 rpm, and there were three gears in the gearbox with a ratio of 1:15. For each working condition, 100 sets of data were collected, and each set of data was collected for 2 s, that is, 40 000 sampling points. After 2 s of each data collection, the setting program of the computer (data receiving terminal) automatically sent out a pop-up window. After the data were confirmed to be correct, it was saved.

The power signals of the TENG and the machinery condition results were displayed in a mobile device via Blyink software. The model of the compressor used in the experiment was EWS30, and the model of the embedded system for data processing was STM32H7.

Supporting Information

Supporting Information is available from the Wiley Online Library or from the author.

Acknowledgements

H.Z., M.S., and Z.A. contributed equally to this work. This work was supported in part by the National Natural Science Foundation of China under Grant Nos. 62104125, 52003141, and 52007019, by the Guangdong Basic and Applied Basic Research Foundation (2020A1515110887), by the Shenzhen Stable Supporting Program (WDZC20200818092033001), by the grant from the Institute for Guo Qiang of Tsinghua University (2020GQG1004), by Tsinghua Shenzhen International Graduate School (HW2021, QD2021013C, QD2021006N, and JC2021007).

Conflict of Interest

The authors declare no conflict of interest.

Data Availability Statement

The data that support the findings of this study are available from the corresponding author upon reasonable request.

Keywords

machinery condition monitoring, self-powered sensors, triboelectric nanogenerators, vibration

Received: April 1, 2022

Revised: July 8, 2022

Published online:

- [1] J. Chen, G. Zhu, W. Yang, Q. Jing, P. Bai, Y. Yang, T. C. Hou, Z. L. Wang, *Adv. Mater.* **2013**, 25, 6094.
- [2] X. Wang, S. Niu, F. Yi, Y. Yin, C. Hao, K. Dai, Y. Zhang, Z. You, Z. L. Wang, *ACS Nano* **2017**, 11, 1728.
- [3] J. Chen, Z. L. Wang, *Joule* **2017**, 1, 480.
- [4] Q. Zhang, K. Barri, S. R. Kari, Z. L. Wang, A. H. Alavi, *Adv. Funct. Mater.* **2021**, 31, 2105825.
- [5] R. Haight, W. Haensch, D. Friedman, *Science* **2016**, 353, 124.

- [6] Z. L. Wang, *Nature* **2017**, 542, 159.
- [7] H. Guo, X. Pu, J. Chen, Y. Meng, M.-H. Yeh, G. Liu, Q. Tang, B. Chen, D. Liu, S. Qi, C. Wu, C. Hu, J. Wang, Z. L. Wang, *Sci. Rob.* **2018**, 3, 2516.
- [8] Z. Wen, M.-H. Yeh, H. Guo, J. Wang, Y. Zi, W. Xu, J. Deng, L. Zhu, X. Wang, C. Hu, L. Zhu, X. Sun, Z. L. Wang, *Sci. Adv.* **2016**, 2, 1600097.
- [9] Y. Zi, J. Wang, S. Wang, S. Li, Z. Wen, H. Guo, Z. L. Wang, *Nat. Commun.* **2016**, 7, 10987.
- [10] Z. L. Wang, *Mater. Today* **2017**, 20, 74.
- [11] J. Cheng, W. Ding, Y. Zi, Y. Lu, L. Ji, F. Liu, C. Wu, Z. L. Wang, *Nat. Commun.* **2018**, 9, 3733.
- [12] J. M. Wu, C. C. Lee, Y. H. Lin, *Nano Energy* **2015**, 14, 102.
- [13] B. Zhang, L. Zhang, W. Deng, L. Jin, F. Chun, H. Pan, B. Gu, H. Zhang, Z. Lv, W. Yang, Z. L. Wang, *ACS Nano* **2017**, 11, 7440.
- [14] R.-j. Yan, S. Pang, H.-b. Sun, Y.-j. Pang, *J. Mar. Sci. Appl.* **2010**, 9, 451.
- [15] C. Wang, X. Zhang, L. Cong, J. Li, J. Zhang, *Evolv. Syst.* **2018**, 10, 649.
- [16] M. Xu, P. Wang, Y.-C. Wang, S. L. Zhang, A. C. Wang, C. Zhang, Z. Wang, X. Pan, Z. L. Wang, *Adv. Energy Mater.* **2018**, 8, 1702432.
- [17] H. Yu, X. He, W. Ding, Y. Hu, D. Yang, S. Lu, C. Wu, H. Zou, R. Liu, C. Lu, Z. L. Wang, *Adv. Energy Mater.* **2017**, 7, 1700565.
- [18] Z. Liu, Y. Zhang, X. Yu, C. Yuan, *Annu. Rev. Control* **2016**, 41, 71.
- [19] Z. L. Wang, *Nano Energy* **2018**, 54, 477.
- [20] W. Ding, J. Zhou, J. Cheng, Z. Wang, H. Guo, C. Wu, S. Xu, Z. Wu, X. Xie, Z. L. Wang, *Adv. Energy Mater.* **2019**, 9, 1901320.
- [21] H. Zhao, M. Xu, M. Shu, J. An, W. Ding, X. Liu, S. Wang, C. Zhao, H. Yu, H. Wang, C. Wang, X. Fu, X. Pan, G. Xie, Z. L. Wang, *Nat. Commun.* **2022**, 13, 3325.
- [22] Z. Tang, S. Lin, Z. L. Wang, *Adv. Mater.* **2021**, 42, 2102886.
- [23] X. Peng, K. Dong, C. Ye, Y. Jiang, S. Zhai, R. Cheng, D. Liu, X. Gao, J. Wang, Z. L. Wang, *Sci. Adv.* **2020**, 6, 9624.
- [24] W. Ding, C. Wu, Y. Zi, H. Zou, J. Wang, J. Cheng, A. C. Wang, Z. L. Wang, *Nano Energy* **2018**, 47, 566.
- [25] C. Wu, W. Ding, R. Liu, J. Wang, A. C. Wang, J. Wang, S. Li, Y. Zi, Z. L. Wang, *Mater. Today* **2018**, 21, 216.
- [26] S. Li, D. Liu, Z. Zhao, L. Zhou, X. Yin, X. Li, Y. Gao, C. Zhang, Q. Zhang, J. Wang, Z. L. Wang, *ACS Nano* **2020**, 14, 2475.
- [27] W. Song, B. Gan, T. Jiang, Y. Zhang, A. Yu, H. Yuan, N. Chen, C. Sun, Z. L. Wang, *ACS Nano* **2016**, 10, 8097.
- [28] X. Meng, Q. Cheng, X. Jiang, Z. Fang, X. Chen, S. Li, C. Li, C. Sun, W. Wang, Z. L. Wang, *Nano Energy* **2018**, 51, 721.
- [29] C. Wu, A. C. Wang, W. Ding, H. Guo, Z. L. Wang, *Adv. Energy Mater.* **2019**, 9, 1802906.
- [30] X. Zhao, G. Wei, X. Li, Y. Qin, D. Xu, W. Tang, H. Yin, X. Wei, L. Jia, *Nano Energy* **2017**, 34, 549.
- [31] S. Wang, S. Niu, J. Yang, L. Lin, Z. L. Wang, *ACS Nano* **2014**, 8, 12004.
- [32] X. Xiao, X. Zhang, S. Wang, H. Ouyang, P. Chen, L. Song, H. Yuan, Y. Ji, P. Wang, Z. Li, M. Xu, Z. L. Wang, *Adv. Energy Mater.* **2019**, 9, 1902460.
- [33] W. Li, Y. Liu, S. Wang, W. Li, G. Liu, J. Zhao, X. Zhang, C. Zhang, *IEEE/ASME Trans. Mechatron.* **2020**, 25, 2188.
- [34] H. Zhao, X. Xiao, P. Xu, T. Zhao, L. Song, X. Pan, J. Mi, M. Xu, Z. L. Wang, *Adv. Energy Mater.* **2019**, 9, 1902824.
- [35] Z. L. Wang, A. C. Wang, *Mater. Today* **2019**, 30, 34.
- [36] J. Wu, X. Wang, H. Li, F. Wang, W. Yang, Y. Hu, *Nano Energy* **2018**, 48, 607.
- [37] W. Yang, J. Chen, G. Zhu, X. Wen, P. Bai, Y. Su, Y. Lin, Z. Wang, *Nano Res.* **2013**, 6, 880.
- [38] Z. Lin, Q. He, Y. Xiao, T. Zhu, J. Yang, C. Sun, Z. Zhou, H. Zhang, Z. Shen, J. Yang, Z. L. Wang, *Adv. Mater. Technol.* **2018**, 3, 1800144.
- [39] C. He, W. Zhu, G. Q. Gu, T. Jiang, L. Xu, B. D. Chen, C. B. Han, D. Li, Z. L. Wang, *Nano Res.* **2017**, 11, 1157.
- [40] T. Bhatta, P. Maharjan, M. Salauddin, M. T. Rahman, S. M. S. Rana, J. Y. Park, *Adv. Funct. Mater.* **2020**, 30, 2003276.

- [41] X. Zhang, J. Zhao, X. Fu, Y. Lin, Y. Qi, H. Zhou, C. Zhang, *Nano Energy* **2022**, 98, 107209.
- [42] H. Wu, J. Wang, Z. Wu, S. Kang, X. Wei, H. Wang, H. Luo, L. Yang, R. Liao, Z. L. Wang, *Adv. Energy Mater.* **2022**, 12, 2103654.
- [43] S. Wang, M. Tian, S. Hu, W. Zhai, G. Zheng, C. Liu, C. Shen, K. Dai, *Nano Energy* **2022**, 97, 107149.
- [44] S.-N. Lai, C.-K. Chang, C.-S. Yang, C.-W. Su, C.-M. Leu, Y.-H. Chu, P.-W. Sha, J. M. Wu, *Nano Energy* **2019**, 60, 715.
- [45] Q. He, Y. Wu, Z. Feng, C. Sun, W. Fan, Z. Zhou, K. Meng, E. Fan, J. Yang, *Nano Energy* **2019**, 59, 689.
- [46] J. Yang, J. Chen, Y. Su, Q. Jing, Z. Li, F. Yi, X. Wen, Z. Wang, Z. L. Wang, *Adv. Mater.* **2015**, 27, 1316.
- [47] W. Zhang, G. Peng, C. Li, Y. Chen, Z. Zhang, *Sensors* **2017**, 17, 425.
- [48] S. R. Saufi, Z. A. B. Ahmad, M. S. Leong, M. H. Lim, *IEEE Trans. Ind. Informat.* **2020**, 16, 6263.